

See discussions, stats, and author profiles for this publication at: <https://www.researchgate.net/publication/278078166>

Potassium-Exchanged Natrolite Under Pressure. Computational Study vs Experiment

ARTICLE *in* THE JOURNAL OF PHYSICAL CHEMISTRY C · SEPTEMBER 2014

Impact Factor: 4.77 · DOI: 10.1021/jp505973r

READS

10

3 AUTHORS, INCLUDING:



Alena Kremleva

Technische Universität München

16 PUBLICATIONS 138 CITATIONS

[SEE PROFILE](#)



Thomas Vogt

University of South Carolina

360 PUBLICATIONS 9,225 CITATIONS

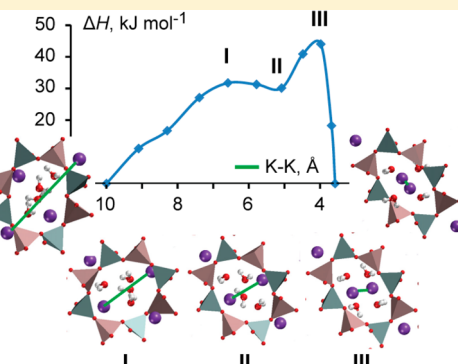
[SEE PROFILE](#)

Potassium-Exchanged Natrolite Under Pressure. Computational Study vs Experiment

Alena Kremleva,[†] Thomas Vogt,[‡] and Notker Rösch*,^{†,§}[†]Department Chemie and Catalysis Research Center, Technische Universität München, 85747 Garching, Germany[‡]NanoCenter & Department of Chemistry & Biochemistry, University of South Carolina, Columbia, South Carolina 29208, United States[§]Institute of High Performance Computing, Agency for Science, Technology and Research, 1 Fusionopolis Way, #16-16 Connexis, Singapore 138632, Singapore

Supporting Information

ABSTRACT: Using density functional theory we modeled the effects of pressure on K-exchanged natrolite, K-NAT, including superhydration and the experimentally observed structural phase transition. Natrolites are composed of T_5O_{10} secondary building units ($T = Si, Al$) linking two Al- and three Si-based TO_4 tetrahedra which in projection have an average chain rotation angle ψ with respect to the crystallographic a - and b -axes. Besides an isomer with pore axes orientations characterized by a negative chain rotation angle, found experimentally at moderate pressure, we also examined a superhydrated isomer with pore axes orientations resulting from positive chain rotation angles in the pressure range 1–2.5 GPa. We estimated the critical pressure for possible transformations between various isomers, but we were unable to identify any specific energetic preference for a superhydrated structure with a negative chain rotation angle. Therefore, our computational results suggest that both isomers coexist in the same pressure range and transform into a more compact structure near 4 GPa. We also modeled the pathways for this latter phase transition and found rather similar barrier heights, 43–44 kJ mol⁻¹ per K⁺ ion for both isomers, but distinct energy profiles. Thus, based on the modeling results, the isomers of superhydrated K-NAT, with either positive or negative chain rotation angles, may coexist at moderate pressures, calling for new experiments.



1. INTRODUCTION

Zeolites are composed of corner-sharing TO_4 -tetrahedra with $T = Si, Al$.^{1,2} An important property of these aluminosilicates is their ability to undergo ion exchange which is exploited in numerous industrial and environmental applications. Natrolite (NAT) ($Na_{16}Al_{16}Si_{24}O_{80} \cdot 16H_2O$) is a naturally occurring small-pore zeolite with an orthorhombic unit cell.^{3,4} It has not been used extensively because of its rather small elliptic pores, less than 4 Å in the small conjugate diameter, which results in steric hindrance for ion exchange. However, recently it was experimentally shown that Na⁺ ions can be fully exchanged by K⁺, and subsequently K⁺ species can be exchanged by other mono- and divalent cations under ambient conditions.^{5,6} Exchange of Na⁺ by K⁺ considerably changes the water–cation configuration in the natrolite channels. Tightly bonded Na⁺ ions and H₂O molecules in Na-NAT convert into a disordered K⁺–H₂O substructure with a different cation–water cluster topology, and the unit cell expands concomitantly. K-NAT, as the first intermediate of ion exchange of Na-NAT, is the main gateway for any exchange of Na⁺ with other cations in a natrolite framework. The convertibility of K-NAT to various mono- and divalent forms is related to the unique structure of its K⁺–H₂O arrangement.⁷

Under moderate pressure, 1–3 GPa, exchanged natrolites were recently found to undergo various structural transformations.^{8–11} The pressure-induced hydration and the resulting cation–water rearrangements were experimentally explored.⁸ Li-, Na-, K-, and Rb-natrolites exhibit superhydration under pressure, while Cs- and K-NAT undergo structural phase transitions. Also, the cations adopt a new structural arrangement inside the natrolite framework.⁸ Very recently, we examined computationally monovalent cation exchange in natrolite at ambient conditions as well as the pressure-induced behavior of Na, Rb, and Cs natrolites. With calculations based on density functional theory (DFT) we were able to reproduce approximately the critical pressure values at which the corresponding transformations were found to occur in experiment.¹² The present computational study addresses the pressure-induced behavior of K-NAT.

The three examples, Na-, Rb-, and Cs-exchanged natrolites, exhibit either one of the basic phenomena that occur under pressure, namely, superhydration and structural phase transition. Rb-NAT under pressure undergoes superhydration in

Received: June 16, 2014

Revised: August 25, 2014

Published: September 10, 2014



one step,^{8,12} whereas pressure-induced insertion of water molecules into Na-NAT occurs in two steps. In the first step hydration is accompanied by a volume increase, while the volume decreases in the second step.^{12–14} Cs-NAT with one aqua ligand per cation in the natrolite framework undergoes a rearrangement of the cation–water structure.^{8,12} Experiments on K-NAT reveal a much more complicated behavior under pressure that combines both types of phenomena.⁸ First of all, the water content of K-NAT at ambient conditions is not defined as precisely as for other exchanged natrolites.⁵ Under moderate pressure, about 1 GPa, K-NAT undergoes superhydration.⁸ At variance with any other ion-exchanged natrolite, insertion of water molecules was reported to be accompanied by an inversion of the channels and negative rotation angle ψ of the T_5O_{10} subunits (see below).⁸ At higher pressure, ~2.5 GPa, superhydrated K-NAT emerges with a new cation–water cluster topology and a positive T_5O_{10} rotation angle ψ .⁸

No such channel inversion or sign change of the chain rotation angle ψ was found in any of the experiments on natrolite and its ion-exchanged congeners. Given the key role of K-NAT in the research on this class of zeolites, it seems important to understand this apparently unique property of K-NAT. To address this more complex behavior of K-NAT under pressure, we elaborated our earlier computational work on K-NAT to the pressure-induced behavior. After examining the structure of “wet” K-NAT at ambient conditions, we modeled the structures of superhydrated K-NAT under pressure. We explored several isomers of superhydrated K-NAT and estimated critical pressure values at which these isomers can transform one into another. To assess the likelihood of such transformations, we also determined the corresponding energy profiles by means of constrained optimizations.

2. COMPUTATIONAL DETAILS

We employed the same computational approach as in our preceding study.¹² We carried out DFT calculations on periodic slab models using the Vienna Ab Initio Simulation Package (VASP).^{15–18} The effect of the core electrons is represented by the full-potential projector augmented wave (PAW) method.^{19,20} We optimized structures with the generalized gradient approximation (GGA) in the form suggested by Perdew, Becke, and Ernzerhof (PBE).^{21,22} The representation in k -space was restricted to the Γ -point. We used a cutoff energy of 520 eV to reduce the effect of Pulay forces during unit cell optimization and to achieve tight convergence of the plane-wave expansion. In geometry optimizations, the total energy was converged to 10^{-6} eV, and forces acting on ions were required to be less than 10^{-4} eV/pm.

The effect of increased pressure on the zeolite structure was modeled by optimizing simultaneously the shape of the unit cell at fixed volume and the positions of ions.¹⁸ The resulting optimized stress tensor exhibited very similar diagonal elements. Therefore, the average of these diagonal elements can be taken to represent the negative of the pressure p , applied to the system. A similar procedure has been used earlier.^{12,23,24} As the plane-wave expansion is not complete with respect to the implied changes of the shape of the unit cell (and its volume when the bulk is optimized), one has to estimate the resulting Pulay stress. Applying the procedure used previously,¹² one estimates an acceptable value, 0.2 GPa, for the pressure uncertainty due to the Pulay stress.

3. RESULTS AND DISCUSSION

It seems useful to recall the main features of the structures of Na- and K-natrolites (Figure 1) as obtained by X-ray powder

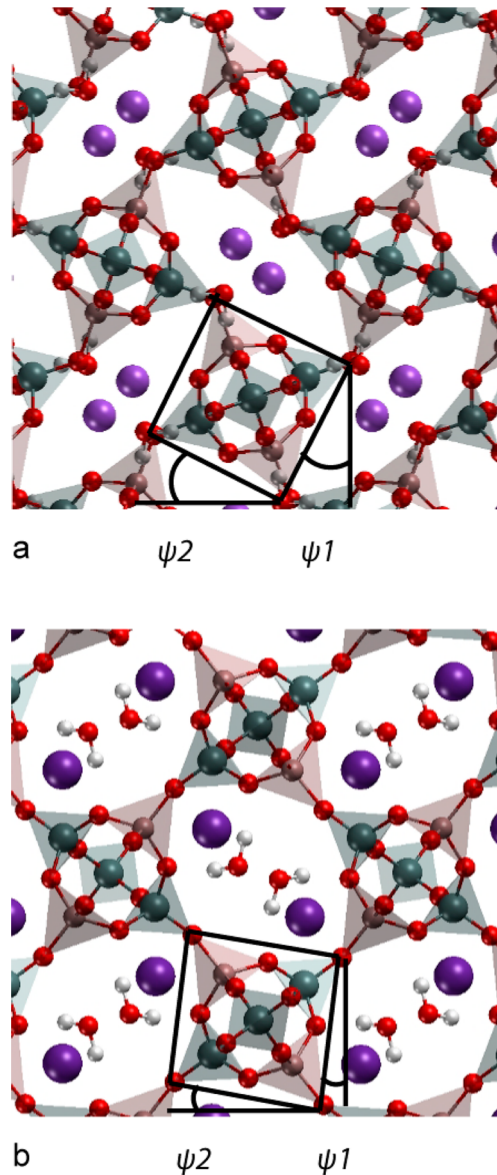


Figure 1. Positioning of nonframework cations and aqua ligands in the zeolite pores at ambient conditions: (a) Na-NAT and (b) K-NAT. The chain rotation angle is defined as $\psi = (\psi_1 + \psi_2)/2$. Both structures are characterized by a positive value ψ of the chain rotation angle.

diffraction.^{5,6} The unit cells exhibit eight channels with two extra-framework cations in each of them. At ambient conditions the unit cell of Na-NAT holds in addition two H_2O ligands per channel. The cations are located close to the axis of the channels along the c direction (Figure 1a) and alternate with water ligands so that each type of species, cations and water molecules, engages in two mutual coordination bonds. The cations also have close contacts to framework O centers. In the channels of K-NAT, ions and water molecules form a zigzag chain, with the cations at corner positions, bridged by O centers of water ligands. Thus, the water ligands are located closer to the channel axis than the cations (Figure 1b). Whereas 16 water molecules per unit cell were experimentally resolved in Na-

Table 1. Data for Lattice Parameters, Calculated at the PBE Level for K-NAT with 24 and 32 H₂O per Unit Cell^a

		isomer	<i>p</i> /GPa	<i>V</i> /Å ³	<i>a</i> /Å	<i>b</i> /Å	<i>c</i> /Å	<i>ψ</i> /°
K-NAT-24	calcd	2a	0.0	2662	19.79	20.49	6.56	6.4
	exptl ^b	1a	0.0	2485	19.34	19.88	6.48	12.5
K-NAT-32	calcd	2b	1.0	2688	19.67	20.72	6.59	-2.8
			2.0	2640	19.51	20.66	6.55	-2.9
	2b*		1.0	2661	19.83	20.25	6.63	9.0
			1.9	2617	19.67	20.16	6.60	10.0
		2c	2.5	2527	19.18	19.81	6.65	16.8
			3.5	2477	19.07	19.59	6.63	17.9
	exptl ^b	1b	1.0	2561	19.97	20.03	6.40	-7.2
			2.0	2520	19.88	19.97	6.35	-5.6
		1c	2.5	2453	19.32	19.60	6.48	17.4
			3.7	2380	19.37	19.11	6.43	19.8

^aThe corresponding experimental data are given for comparison. For designation of isomers see Figure 2. ^bRef 8.

Table 2. Contacts (Å) of Ions K⁺ to O Centers of Aqua Ligands, K–O_{aq}, and to O Centers of the Zeolite Frame, K–On, *n* = 1–5, from Calculations at the PBE Level of Theory^a

model	structure	<i>p</i> /GPa	K–O _{aq}	K–O1	K–O2	K–O3	K–O4	K–O5
K-NAT-24	calcd 2a	0.0	2.89 (x2), 2.76	3.06	3.16	3.00	3.02	2.90
	exptl ^b K1	0.0	2.39/3.07 ^c , 2.68	2.85		2.82	2.86	2.89
	exptl ^b K2	0.0	3.07/2.40 ^c , 3.14			2.94	2.92	2.76
K-NAT-32	calcd 2b	1.0	2.83, 2.83, 3.13	2.87	3.07	3.19	3.16	2.94
	calcd 2b*	1.0	2.72, 2.97, 3.34	3.05		3.04	2.99	2.99
	exptl ^b 1b	1.0	2.63, 2.63, 2.93	2.96	3.24	3.25	2.92	3.02
K-NAT-32	calcd 2c	3.5	2.64, 2.64, 2.73		2.79, 3.04	2.71	2.74	
	exptl ^b 1c	3.7	2.65, 2.76, 2.89		2.82, 2.83	2.66	2.57	

^aFor designation of isomers see Figure 2. ^bRef 8. ^cTwo positions, OW1 and OW2, of aqua ligands resolved in experiment; the first distance given corresponds to the bonds K1–OW1 and the second to the K1–OW2 bonds, and similarly for K2 positions.

NAT,¹⁴ the water content of K-NAT is less certain. In experiment, “dry” K-NAT was determined to feature 14 H₂O per unit cell, while the “wet” isomer, resulting from soaking K-NAT in water, comprises 22 H₂O per unit cell.⁵ For the sake of a more consistent comparison with other exchanged natrolites, we modeled “dry” and “wet” isomers of K-NAT by 16 and 24 water molecules per unit cell, to be referred to as K-NAT-16 and K-NAT-24, respectively. Previously we addressed “dry” K-NAT at ambient conditions.¹² The present work explores “wet” K-NAT as it serves as the initial structure for pressure-induced hydration. X-NAT-*n* will designate a compound of X-exchanged natrolite with *n* water molecules per unit cell.

3.1. Structure Parameters of “Wet” K-NAT at Ambient Conditions. Table 1 shows the optimized unit cell parameters of K-NAT-24 and the corresponding experimental data of “wet” K-NAT at ambient conditions. We started the geometry optimization with this experimental structure, maintaining the orthorhombic shape of the unit cell. The unit cell parameters calculated at the GGA level overestimate the experimental values, at most by 0.6 Å (3%) for the unit cell parameters *a* and *b* and by 0.1 Å (2%) for vector *c*. Similar results were calculated earlier for other monovalent exchanged natrolites.¹² The overall volume of the unit cell was computed 177 Å³ larger than the experimental volume; this overestimation of the experimental value is somewhat larger, by ~80 Å³, than for the other exchanged natrolites.¹² Another important characteristic of the natrolite framework is the T₅O₁₀ chain rotation angle *ψ*; for a definition, see Figure 1 and ref 12. This angle reflects the opening of the channels: smaller *ψ* (<15° in absolute value) corresponds to widely open channels, while larger values of *ψ* (~25° for Na-NAT) signal a compact structure with closed

channels. In experiment, angles *ψ* are determined to ~13° at ambient conditions, for both “dry” and “wet” K-NAT.⁸ The angles were calculated at 16° and 6° for K-NAT-16 and K-NAT-24, respectively. Experimentally, no large changes of the volume and the chain rotation were noted when “dry” K-NAT takes up water, to become “wet”.⁸ Computationally the volume increases by ~130 Å³, and the chain rotation angle decreases by 10°. This disagreement between experimental and computational results may be attributed either to inaccuracies in the diffraction experiments and the determination of the water content or to the lack of thermal perturbations in the computational approach.

To evaluate the interaction of the cations in the channels with the water molecules or framework oxygen centers, we collected the pertinent cation–water K–O_{aq} and cation–framework oxygen K–O_{fr} distances in Table 2. The natrolite lattice exhibits only five symmetry-nonequivalent framework oxygen centers, the labels of which are defined in the Supporting Information (SI) of our earlier study.¹² Experimentally positions of K⁺ ions were resolved for “wet” K-NAT, labeled K1 and K2 in Table 2. K⁺ ions occupying the first position exhibit four contacts to the framework and three contacts to aqua ligands, while in the second position they are only 3-fold coordinated to the framework and exhibit three contacts to H₂O (Table 2). In our calculations, we were able to determine only a single position for K cations. Each K⁺ of the optimized structure of K-NAT-24 shows five contacts of about the same lengths to the framework O centers, 2.90–3.16 Å, with the longest contact to the O2 center, which is missing in the experimental data (Table 2). Coordinative K–O_{aq} bonds to aqua ligands were calculated at 2.76–2.89 Å, i.e., slightly shorter

than the bonds to the framework oxygen centers. The optimized structure of “wet” K-NAT agrees better with the experimental ion position K1 (Table 2), which, given its occupancy of 0.59,⁸ is the most probable structure resolved in the experiment.

3.2. Pressure-Induced Hydration of K-NAT. Experiments on the superhydration of K-NAT showed that the water content of the unit cell of K-NAT increases to 32 H₂O molecules at ~1 GPa.⁸ This change is accompanied by a sign change of the chain rotation angle ψ of K-NAT (Figure 2, structure 1b):⁸ the major axes of the natrolite channels are interchanged, and a negative chain rotation angle, $\psi = -7.2^\circ$ is observed (Table 1). At ~2.5 GPa the angle ψ reverts back to a positive value, and the major axes of the channels interchange again as does the arrangement of cations and water ligands which transforms to a denser structure as observed in Na-NAT-32 (Figure 2, structure 1c).⁸ Thus, in the absence of any other cations for exchange, K-NAT under pressure undergoes transformations from structure 1a to 1b to 1c, respectively (Figure 3).

No sign change of ψ was observed for any other exchanged natrolites.^{8,9,11,14} Small rotation angles correspond to wider channels, and $\psi = 0$ entails channels with essentially round cross sections, i.e., with minor and major axes being similar. This is where the volume of the channels and the unit cell are expected to be close to maximum. Thus, to reach negative values of ψ (Table 1), the channels first have to open significantly, before major and minor axes of the channels exchange and ψ becomes negative. Hence, sign changes of ψ should be easier for structures with smaller values of ψ .

The volume of the natrolite channels and therefore the volume of the unit cell correlate with the ionic radii of the nonframework cations; for data of systems at ambient conditions, see Figure 1 of ref 12. Rb-NAT is the monovalent exchanged natrolite that is most similar to K-NAT as their ionic radii are rather similar: K⁺, 1.52 Å; Rb⁺, 1.66 Å.²⁵ Although superhydration to 32 H₂O molecules per unit cell occurs at different pressure values, ~1 GPa for K-NAT and ~2 GPa for Rb-NAT, the chain rotation angles of both K-NAT and Rb-NAT before superhydration are very similar, 12.5 and 12.1°, respectively,⁸ as are the final volumes of the corresponding superhydrated structures with 2560 (Table 1) and 2587 Å³, respectively.⁸ Thus, channels have to be widely open during superhydration in both K-NAT and Rb-NAT. However, after pressure-induced superhydration, only K-NAT-32 is experimentally observed to have a negative ψ , whereas Rb-NAT-32 has not.⁸

Therefore, one may hypothesize that superhydrated K-NAT-32 might simultaneously have two isomers, one with a negative chain rotation angle, ψ_- , and the other with a regular positive angle, ψ_+ , with similar arrangements of the water–cation chains at similar pressure conditions. We optimized the structure of these two isomers of superhydrated K-NAT-32 in the pressure range 1–2.5 GPa (Figure 2): (i) The initial configuration for optimizing structure 2b* was constructed by simply inserting eight more water molecules into K-NAT-24; (ii) structure 2b with ψ_- was modeled after the experimental structure.⁸ We also examined an isomer of K-NAT-32 with the cation–water arrangement of Na-NAT-32 as it is observed for K-NAT-32 in experiments at p above 2.5 GPa (structure 2c, Figure 2).

Next, we compare the geometric parameters of the optimized structures to data from experiment (Tables 1 and 2). At all pressures examined, the calculated unit cell volumes of all three

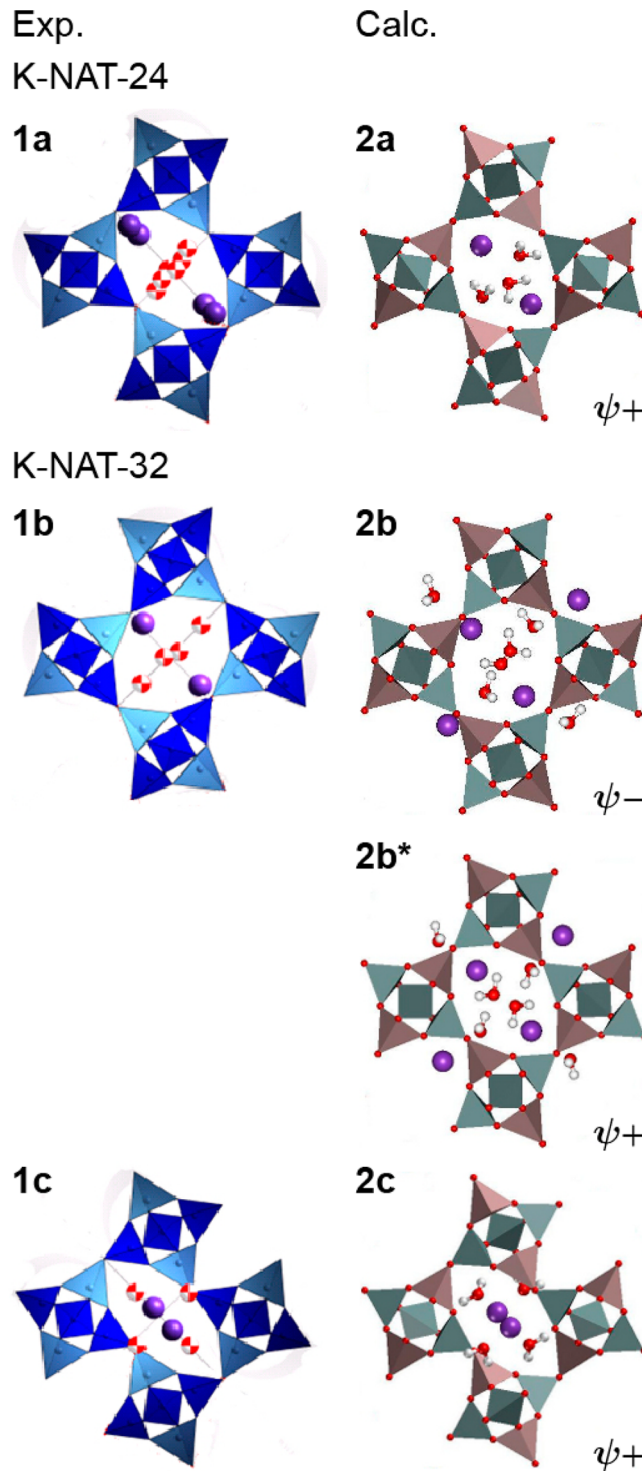


Figure 2. Schematic representation of various isomers of K-NAT under pressure. The left-hand column represents experimentally observed isomers (adapted from ref 8), and the right-hand column shows results of computational modeling. The appropriate chain rotation angles ψ_+ and ψ_- are also indicated.

structures of the three isomers of K-NAT-32 overestimate the corresponding experimental values by 100–120 Å³. Such a small overestimation, less than 5%, was found typical at the PBE level of theory for exchanged natrolites at ambient conditions.¹² An empirical correction for van der Waals interactions^{12,26} improves the agreement between computed

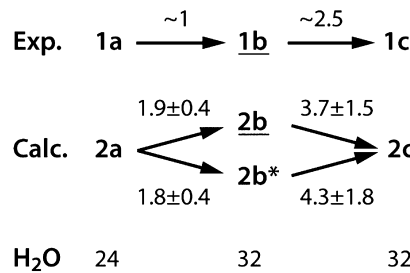


Figure 3. Schematic representation comparing experimental and calculated pressure-induced transformations in K-NAT. Values at the arrows indicate the critical pressure p^* (GPa) at which the phase transition occurs. For the designation of the isomers, see Figure 2; labels of isomer with a negative ψ are underlined. The number of water molecules per unit cell is also indicated; in experiment the water content of isomer 1a is 22 (see text).

and experimental volumes at ambient conditions but fails to reproduce the experimental behavior under pressure.¹²

The present PBE results reproduce quite well qualitative trends of the p - V diagram (Figure 4). When structure 2a

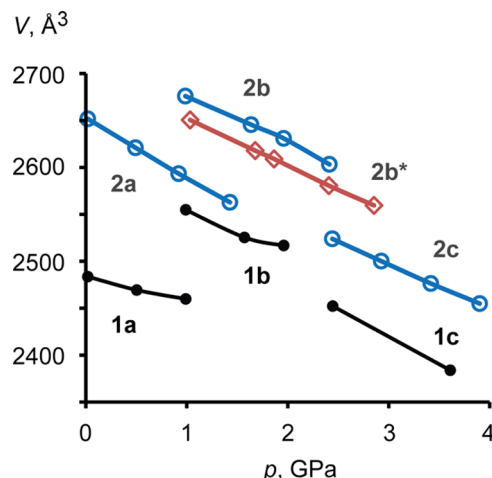


Figure 4. p - V diagram from PBE calculations for K-NAT. Experimental data from ref 8 for the structures 1a (K-NAT-24, $\psi+$), 1b (K-NAT-32, $\psi-$), and 1c (K-NAT-32, $\psi+$) are shown as black dots. The calculated results are shown as blue empty circles for the structures 2a (K-NAT-24, $\psi+$), 2b (K-NAT-32, $\psi-$), and 2c (K-NAT-32, $\psi+$), and as red empty diamonds for isomer 2b* (K-NAT-32, $\psi+$). For details see text and Figure 2.

undergoes superhydration at ~ 1 GPa to structures 2b or 2b*, the volume V of the unit cell is calculated to increase, but both optimized structures 2b and 2b* feature decreasing volumes when converting into a structure of type 2c at higher pressure, 2.5 GPa (Figure 4). The volume $V(2b)$ of isomer 2b is slightly larger than $V(2b^*)$. However, this difference in volume is still smaller than the volume increase/decrease due to pressure-induced superhydration or structural phase transition; see the jumps in Figure 4 at 1 GPa and at 2.5 GPa, respectively.

To discuss pressure effects on the structures in more detail, we now turn to the K–O distances in the calculated structures of K-NAT-32. We compare the coordination of ions by both framework oxygen centers and aqua ligands and compare it to experimental results (Table 2).⁸ As these structures are not available at ambient conditions, we will carry out this

comparison at $p = 1$ GPa for isomers 2b and 2b* and at $p \approx 3.5$ GPa for isomer 2c.

At 1 GPa, the cations in the experimentally found K-NAT structure have three K–O_{aq} contacts (2.63, 2.63, and 2.93 Å) and five K–O_{fr} (2.92–3.25 Å; see Table 2, structure 1b), thus a total coordination number of 8. For isomer 2b, with a $\psi-$, we determined also three K–O_{aq} contacts to water ligands (2.83, 2.83, and 3.13 Å; Table 2). These contacts typically are by ~ 0.2 Å longer than the corresponding experimental distances of structure 1b. The five K–O_{fr} distances of structure 2b vary from 2.87 to 3.19 Å (Table 2); on average, they are ~ 0.1 Å shorter than the corresponding experimental distances, with the exception of contact K–O4 which is calculated to be 0.24 Å longer. Thus, with an uncertainty of ~ 0.2 Å, isomer 2b reproduces the experimental structure 1b rather well. Isomer 2b* agrees less well with the experimental structure 1b, as it reveals only 7 K–O contacts, and the distances K–O_{aq} are considerably longer, by 0.3–0.4 Å, compared with the experimental data (Table 2). Isomer 2b was initially constructed from experimental data;⁸ thus it is expected to have a structure closer to the experiment than isomer 2b*, the optimization of which was started from an “assumed” structure.

The experimental structure⁸ 1c (Figure 2) of K-NAT at 3.7 GPa features three K–O_{aq} bonds with aqua ligands and 4 K–O_{fr} contacts to the framework, all seven varying from 2.57 to 2.89 Å (Table 2). The ion–water arrangement of that structure resembles that determined experimentally⁸ for Na-NAT, where the cations are located close to the center of the channel, alternating with aqua ligands along vector c of the unit cell. Just as Na-NAT,¹² the cations in K-NAT exhibit two contacts to O2 centers, 2.82 and 2.83 Å, and in addition one to O3, 2.66 Å, and one to O4, 2.57 Å (Table 2). Largely similar results are obtained for the optimized isomer 2c: three K–O_{aq} contacts, only slightly shorter than the experimental values K–O_{aq}, and 4 K–O_{fr} coordination bonds in the same fashion, two bonds to O2, one to O3, and one to O4. The calculated distances K–O_{fr} are in general longer than those determined experimentally (Table 2). However, within an average deviation of ~ 0.15 Å, the computational results for the compact form 2c of K-NAT-32 at $p \approx 3.5$ GPa agree very well with the corresponding experimental data, structure 1c.

3.3. Critical Pressure Values. Now, we will estimate the critical pressure for the transformations of structure 2a to structures 2b/2b* and subsequently to the isomer 2c. To estimate the pressure p^* at which superhydration (or structural phase transition) occurs in K-NAT, one needs to determine when the enthalpy change $\Delta H(p)$ of the following reactions is zero



Equation 1 represents superhydration, and the second (eq 2) corresponds to the structural phase transition between isomers X and Y. We approximate the enthalpy as $H(p) = U(p) + pV$.¹² The enthalpy of bulk water is estimated by optimizing the structure of a unit cell with 16 H₂O at pressure values up to 2.5 GPa. For solving the equation $\Delta H(p^*) = 0$, we represented all values $H(p)$ by linear fits in p . All pertinent data are given in the SI. The procedure for estimating the uncertainties is described in detail in the SI of ref 12. The resulting critical pressure values p^* are shown in Figure 3.

The calculated critical pressure values for the superhydration of K-NAT-24 (**2a**) are 1.9 ± 0.4 GPa for isomer **2b** with ψ^- and 1.8 ± 0.4 GPa for isomer **2b*** with ψ^+ . Superhydration with ψ^+ structure (**2b***) is computationally predicted to occur slightly “earlier”, at 1.8 GPa compared to 1.9 GPa, estimated for superhydration accompanied by a ψ^- (**2b**). However, taking into account the uncertainty of 0.4 GPa, it does not seem appropriate to interpret the difference of 0.1 GPa. Both calculated values of the critical pressure p^* overestimate the corresponding experimental result, ~ 1 GPa, by about 1 GPa. Yet, this is in line with the quality of our previous results for other natrolite compounds with exchanged monovalent ions.¹² In this context, lack of entropic contributions and other temperature effects may play a role, yet to be assessed.

According to our calculations, structures with ψ^- do not have any notable energetic advantages. Of course, one can also directly compare the total enthalpy values $H(p)$ of the two isomers, **2b** and **2b***, at the same pressure values. At 1 GPa, isomer **2b*** is 7 kJ mol⁻¹ per unit cell more favorable than isomer **2b**. At 2 GPa this difference increases to 14 kJ mol⁻¹ and at 3 GPa to 19 kJ mol⁻¹ per unit cell. Thus, between 1 and 3 GPa isomer **2b*** is slightly more favorable than structure **2b** with a ψ^- . However, this energy preference never exceeds 1.2 kJ mol⁻¹ per K⁺ ion. Such small energy differences between two isomers may be taken as a hint for their possible coexistence.

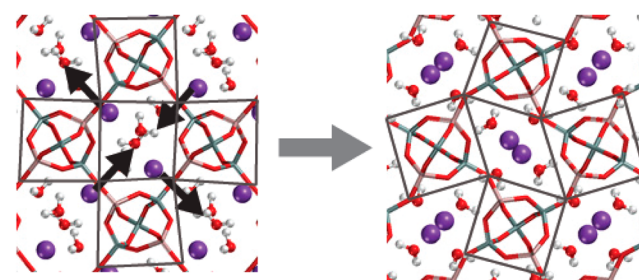
We also estimated the critical pressure p^* for the subsequent structural phase transition for the isomers **2b** and **2b***. According to our models, the phase transition of isomer **2b** to the more compact isomer **2c** is expected to happen at 3.7 ± 1.5 GPa, while isomer **2b*** was estimated to transfer into **2c** at 4.3 ± 1.8 GPa (Figure 3). The critical pressure p^* of a structural phase transition, eq 2, is expected to be reproduced better than the critical pressure for superhydration, eq 1, from 24 to 32 H₂O molecules per unit cell. After all, when the number of water molecules per unit cell does not change, the corresponding entropy effects can be assumed to cancel. For the structural phase transition in Cs-NAT, the computationally predicted pressure 1 ± 0.7 GPa¹² agrees quite well with the experimental value, 0.3–1.5 GPa.⁸ However, the experimental value, ~ 2.5 GPa,⁸ for the pressure at which the structural phase transition occurs in K-NAT is at the edge of the regions estimated for p^* from computational results, 2.2–5.2 GPa for isomer **2b** and 2.5–6.1 GPa for isomer **2b***. Also, the standard deviations estimated for the critical pressure p^* are quite large, 1.5 and 1.8 GPa (Figure 3). In short, from our modeling results, it is hard to assess which of the isomers, **2b** or **2b***, transforms more easily into isomer **2c**.

To put the accuracy of the present results into perspective, recall that our computational approach very well reproduces qualitative trends for various monovalent exchanged natrolites.¹² The first step of Na-NAT superhydration and superhydration of K-NAT were measured to occur at ~ 1 GPa and predicted computationally for pressure values of 1.8–2.3 GPa. The second step of superhydration of Na-NAT, experimentally found to occur between 1 and 1.5 GPa, was computationally predicted at 2.4 GPa. Superhydration of Rb-NAT, determined to occur in experiment at 1.7–2.0 GPa, was predicted computationally at 2.7 GPa.¹² The structural phase transition for K-NAT was computationally predicted to occur near 4 GPa, while in experiment the phase transition for K-NAT was observed at approximately 2.5 GPa.

3.4. Structural Phase Transitions. To understand better the structural phase transition of K-NAT and, in particular, the

possibility for coexistence of isomers, we went on to explore pathways of structure changes involved in the phase transitions **2b** \rightarrow **2c** at $p = 3.7$ GPa and **2b*** \rightarrow **2c** at $p = 4.3$ GPa. The main effect of the structural phase transition in both cases is a rearrangement of K⁺ cations that leads to a concomitant rearrangement of water molecules and triggers subsequent changes of the natrolite framework. We assumed that K⁺ ions slip through the smaller pores, which connect the channels, from one channel into a neighboring one. Figure 5 sketches the

2b \rightarrow **2c**



2b* \rightarrow **2c**

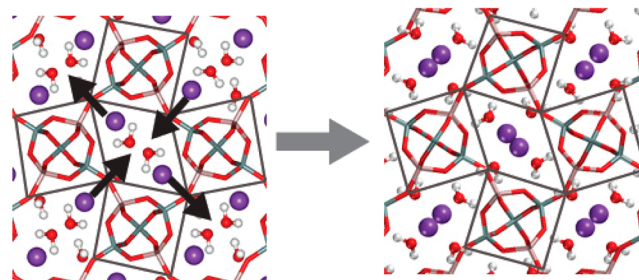


Figure 5. Structure changes during the phase transitions of K-NAT-32, **2b** \rightarrow **2c** and **2b*** \rightarrow **2c**, under pressure $p = 3.7$ and 4.3 GPa, respectively. Suggested structure change from low to high pressure; black arrows indicate the directions of motion of the cations.

suggested pathways. A similar scenario was proposed for the structural phase transition occurring in Cs-NAT-16,¹² where we had calculated an enthalpy barrier of only 45 kJ mol⁻¹ per Cs⁺ along a linear synchronous transit pathway^{27,28} that connects the initial and final states. The maximum enthalpy was located when the Cs cations were located in the small pores of Cs-NAT-16, about halfway between the two neighboring channels.¹²

The same type of pathway seems to be possible in the case of K-NAT. Initially the cations are at the far ends of the major axis of the elliptical channels. After slipping through the small pores they appear on the minor axis of the neighboring channels. This way, they migrate closer to the center of the channel, and the ion–water network there can transform into a more dense arrangement, similar to the one found in Na-NAT. To model this pathway we constructed nine intermediate sets of K⁺ coordinates as done previously for Cs-NAT-16.¹² For each intermediate geometry, we carried out constrained optimizations of the volume of the unit cell and the positions of the atoms, while keeping the positions of the 16 K cations fixed. The resulting enthalpy profiles in terms of relative enthalpy changes per K⁺ are shown in Figure 6. Figure 7 illustrates the structures of the involved stationary points.

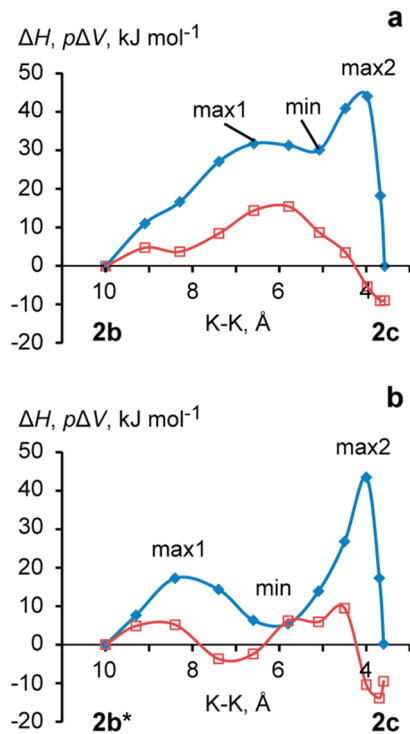


Figure 6. Calculated enthalpy variation ΔH (filled diamonds, blue curve) along a linear synchronous transit path that connects the two isomers at fixed pressure. The effect of the term $\Delta H - \Delta U = \Delta(pV) = p\Delta V$, as the difference between enthalpy H and energy U , is shown separately (open squares, red curve). (a) Phase transition of K-NAT-32, **2b** \rightarrow **2c**, under pressure 3.7 GPa. (b) Phase transition of K-NAT-32, **2b*** \rightarrow **2c**, under pressure 4.3 GPa.

We first discuss the enthalpy profile associated with the structural phase transition **2b** \rightarrow **2c** at $p = 3.7$ GPa (Figure 6a; Figure 7, upper row of panels). The first barrier of the profile, marked as “max1”, corresponds to the structure with a ψ^- , whereas already the structure corresponding to the next point on the path resembles the structure with a ψ^+ . The inversion of the channel occurs between the structures max1 and min

(Figure 7, upper row); the longer axes of these elliptical channel cross sections appear vertically inverted. Intermediate stationary points along each path are approximated by the nearest structures calculated. Thus, the first barrier, 32 kJ mol⁻¹ per ion, is associated with the inversion of the channels. The second barrier is notably higher, 44 kJ mol⁻¹ per ion, and is followed by a rather abrupt descent of the profile to the final state. This second barrier corresponds to major changes in the K⁺–water network inside the channels where K–O_{fr} bonds to the framework are broken and formed. Characteristic K–O distances of the various structures, corresponding to the stationary points max1, min, max2, and the final structure **2c**, are given in Table 3. In the structure min, a total four contacts of K⁺ to aqua ligands can be seen, whereas the structure max2 is characterized by only three K–O_{aq} contacts. In addition, the bonds K–O1 and K–O5 are broken when going from min to max2 (Table 3). These structure changes resulted in an enthalpy increase of 14 kJ mol⁻¹ relative to the structure min (Table 3). Relative to structure max2, the final structure **2c**, at 3.7 GPa, is characterized by all K–O_{aq} bonds becoming shorter, hence stronger; also an additional bond to the framework center O2 is formed (Table 3).

To assess how the difference $\Delta H - \Delta U = \Delta(pV)$ between enthalpy and energy evolves along the path studied, we discuss the change $\Delta(pV) = p\Delta V$ at constant pressure due to the change in volume of the unit cell (Figure 6a). For the most part of the path this term has a destabilizing effect with regard to the energy U which is largest in the section of the path between max1 and min, where the inversion of the unit cell occurs, i.e., for K–K distances from 6.6 and 5.8 Å. The pV term increases the first barrier, max1, by 15 kJ mol⁻¹. Only toward the end of the path is the pV term slightly stabilizing the enthalpy of the system. However, it counteracts the energy contribution by only 5 kJ mol⁻¹ to yield the enthalpy barrier max2. The enthalpy profile (Figure 6a) is notably affected by the increase in volume of the unit cell with a negative chain rotation ψ^- .

Figure 6b shows the enthalpy profile for the analogous transition between K-NAT-32 isomers **2b*** and **2c** at $p = 4.3$ GPa. Figure 7 (lower row) illustrates the structural changes along the enthalpy profile within a single channel. The enthalpy

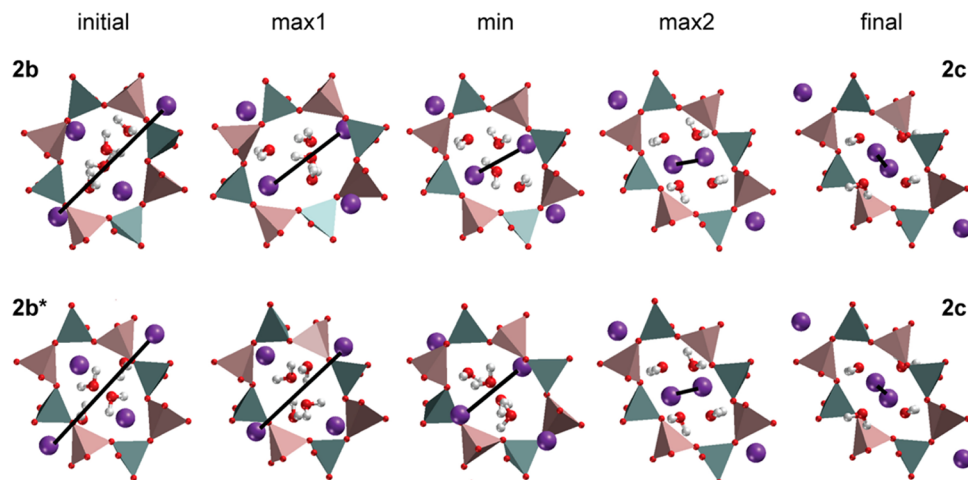


Figure 7. Sketches of atomic positions at the stationary points of the enthalpy profiles for the pathways that represent the modeled phase transition: upper panel, **2b** \rightarrow **2c** transition at $p = 3.7$ GPa, see Figure 6a; lower panel, **2b*** \rightarrow **2c** transition at $p = 4.3$ GPa, see Figure 6b. The black lines indicate the K–K distance, chosen as a reaction coordinate; see Figure 6. Although the two structures in the last column seem visually indistinguishable, they represent isomer **2c** of K-NAT-32 at different pressure values.

Table 3. Characteristic Parameters of Key Structures^a Along the Pathways Modeled to Represent the Phase Transitions **2b → **2c** and **2b*** → **2c** of K-NAT-32 (see Figure 6) at Fixed Pressure Values $p = 3.7$ GPa and $p = 4.3$ GPa, Respectively^b**

pathway		ΔH	K–O _{aq1} ^c	K–O _{aq2} ^c	K–O1	K–O2	K–O3	K–O4	K–O5
2b → 2c	initial	0	2.78	2.79, 3.04	2.92	3.18	3.03	3.01	2.95
	max1	32	2.73	2.90, 2.90	2.94	2.85	2.81 ^c	2.87 ^c	2.96
	min	30	2.73, 2.73	3.01, 3.01	2.87 ^c	2.67	2.70 ^c	2.84	3.03
	max2	44	2.73, 2.73	2.75		2.67	2.87	2.67 ^c	
	final	0	2.64, 2.64	2.73		2.79, 3.03	2.71	2.74	
2b* → 2c	initial	0	2.70, 3.29	2.89, 3.32	3.00		2.89	2.87	2.93
	max1	17	2.73, 2.73		2.80	3.26	2.98	2.82	2.81
	min	6	2.70, 3.22	2.79, 3.24	2.90	3.02	2.87 ^c	2.91 ^c	2.91
	max2	43	2.45, 2.96	2.74		2.71	2.92	2.65 ^c	
	final	0	2.64, 2.64	2.73		2.79, 3.03	2.71	2.74	

^aAlong each path, initial state, first maximum, minimum, second maximum, and final state; see Figures 6a and 6b. Intermediate stationary points along each path are approximated by the nearest structures calculated. ^bRelative enthalpy changes ΔH (kJ mol⁻¹) per K⁺ cation; contacts K–O_{aq1} and K–O_{aq2} (Å) of ions K⁺ to O centers of aqua ligands; contacts K–On, n = 1–5, to O centers of the zeolite frame. ^cOnly 8 out of 16 K⁺ ions in the unit cell are coordinated to the framework centers mentioned.

profile has a double-hump structure with barrier heights of 17 and 43 kJ mol⁻¹ per ion. In contrast to the **2b** → **2c** transition, both barriers are associated with rearrangements of the network of K cations and aqua ligands and the subsequent breaking/forming of K–O_{fr} bonds (Table 3). The first, lower barrier max1, corresponds to the breaking of two coordinative bonds between K⁺ and aqua ligands (Table 3) and the formation of a rather weak bond to framework centers O2, at 3.26 Å. At the local enthalpy minimum min, a structure is present where the K cations form new bonds K–O_{aq} with aqua ligands in neighboring channels. The second barrier of 43 kJ mol⁻¹ in the enthalpy profile corresponds to the rearrangement of K cations and aqua ligands within a channel to adopt the compact structure of isomer **2c**. On the way from the structure min to the structure max2, K contacts to O1 and O5 are lost (Table 3). Note that in structure max2 only three K–O_{aq} are observed, compared to four such contacts in structure min. All these rearrangements induce an enthalpy change of 43 kJ mol⁻¹ relative to the initial and final states (Table 3). The enthalpy change from the highest barrier to the final state is again rather abrupt, as for the transition **2b** → **2c**. In the final state, isomer **2c**, one has four bonds to framework oxygen centers, one more than in the structure max2, and three rather short K–O_{aq} bonds.

The effect of the pV term in this case is less pronounced than in the **2b** → **2c** transition. The pV term stabilizes the second barrier by 14 kJ mol⁻¹, while the structure min is destabilized by 6 kJ mol⁻¹. The changes of the volume along the path do not exceed 2%, and this finding seems to rationalize why the path is not that sensitive to the pressure. To check this we modeled the same path at fixed $p = 3.7$ GPa. As a result, the relative enthalpy values changed at most by 3 kJ mol⁻¹ (at structure min), and barrier heights changed by at most 1 kJ mol⁻¹. If one assumes that the volume changes are very similar at the two pressure values, 3.7 and 4.3 GPa, one can also estimate the effect of the term pV on ΔH as $\Delta p \times \Delta V$. The ΔH values obtained in this way agree within 2 kJ mol⁻¹ per K ion with the enthalpy profile calculated directly at $p = 3.7$ GPa.

In contrast to Cs-NAT, the K-NAT structure with K located in the middle of the small pores does not correspond to an enthalpy maximum along the transition path, in neither **2b** → **2c** nor **2b*** → **2c** (Figures 6 and 7). Potassium cations have much smaller ionic radii, 1.52 Å, compared to Cs⁺, 1.81 Å.²⁵ Therefore, one expects that it is much easier for K cations to slip through the small pores than for Cs ions.

For both enthalpy profiles of K-NAT-32, **2b** → **2c** and **2b*** → **2c**, the highest barriers are very similar, 44 and 43 kJ mol⁻¹ per ion, respectively. These barriers are also similar to the one we calculated for the profile characterizing the structural phase transition of Cs-NAT, 45 kJ mol⁻¹.¹² It seems fortuitous that all three barriers are calculated to be very similar because the structures at the maxima of the barriers are quite different in these three cases as are the overall structure changes from initial to final states. Recall also that Cs-NAT exhibits 16 H₂O per unit cell while K-NAT has 32 aqua ligands. Thus, for K-NAT additional energy is required to rearrange the ion–water network in the channels, whereas for Cs-NAT the main barrier occurs when bulky Cs cations slip through the pores. On the basis of the present enthalpy profiles, one expects that also the transition **2b*** → **2c**, not observed yet in experiments on K-NAT-32, is energetically reasonable.

4. CONCLUSIONS

Addressing the pressure-induced behavior of K-NAT, the present study extended our modeling of monovalent exchanged natrolites under pressure.¹² According to experiments,⁸ K-NAT, partially hydrated already at ambient conditions, undergoes (i) superhydration at ~1 GPa accompanied by a negative chain angle rotation ψ_- and (ii) a structural phase transition concomitant with a restoration of the original positive chain rotation angle at ~2.5 GPa. Among all natrolites exchanged with monovalent ions,^{8–10} only experiments on K-NAT⁸ in pure water medium showed a ψ_- , i.e., an exchange of the major axes of the natrolite channels. With our DFT modeling we explored structures of “wet” potassium exchanged natrolite (K-NAT-24, ambient conditions, **2a**) and superhydrated K-NAT-32 ($p \approx 1$ –3 GPa), the latter with both inverted (**2b**, ψ_-) and noninverted channels (**2b***, ψ_+). In addition, we examined a path that models the structure change during the structural phase transition of K-NAT-32 at higher pressure values, where K cations are located closer to the center of the natrolite channels, thus forming a denser structure (**2c**). The values estimated for the two isomers are rather similar: the critical pressure for the superhydration of K-NAT is predicted to occur at 1.9 GPa (**2b**) and 1.8 GPa (**2b***). The models also forecast the subsequent phase transition to the denser structure **2c** at 3.7 and 4.3 GPa, respectively. As in our previous modeling of ion-exchanged natrolites,¹² the calculated pressure values notably overestimate the corresponding situations in experi-

ment, by 1 GPa and more. Yet, the calculated structures compare well with experimental data. All evidence from the present modeling suggests that superhydrated K-NAT-32 may exist in the form of two isomers, with both inverted and normal channels in the unit cell. Thus far, experiments have revealed only the former structure. Comparison of the total energies shows a very small preference, at most 1.2 kJ mol^{-1} per K^+ ion, for structure **2b*** with a positive chain rotation angle $\psi+$.

We also modeled possible pathways for both structural phase transitions, **2b** \rightarrow **2c** and **2b*** \rightarrow **2c**, by means of constrained optimization. The energy profile of transition **2b** \rightarrow **2c** revealed a two-step shape, with the corresponding heights of enthalpy barriers of 32 and 44 kJ mol^{-1} , relative to the structures at either end of the pathway. The profile of transition **2b*** \rightarrow **2c** was calculated to show a double-hump shape with two distinct enthalpy barriers of 17 and 43 kJ mol^{-1} . The latter phase transition under higher pressure values, from the structure with a $\psi-$ to the denser structure with a $\psi+$, seems to be "kinetically" equally feasible. The highest enthalpy barriers of either path are slightly lower than the barrier for the structural phase transition of Cs-NAT, estimated at 45 kJ mol^{-1} .¹²

In summary, both isomers of superhydrated K-NAT, **2b** and **2b***, were calculated to have similar total energies and energy barriers. Therefore, the present modeling suggests that the isomers are thermodynamically and kinetically similar in the same pressure range, from ~ 2 to ~ 4 GPa. Hence, these isomers may even coexist in experiment, in the pressure range from 1 to 2.5 GPa, where thus far only isomer **1b** of K-NAT has been observed.

ASSOCIATED CONTENT

Supporting Information

Data for the p - V diagrams, data of linear fits of the enthalpy $H(p)$ as a function of pressure p , and data for the modeled pathways of the structural phase transitions, including schematic pictures of the structures at stationary points of these graphs. Coordinates of the optimized structures. This material is available free of charge via the Internet at <http://pubs.acs.org>.

AUTHOR INFORMATION

Corresponding Author

*E-mail: roesch@mytum.de.

Notes

The authors declare no competing financial interest.

ACKNOWLEDGMENTS

The authors gratefully acknowledge a generous grant of computing resources by the Gauss Centre for Supercomputing (www.gauss-centre.eu), provided on the SuperMUC platform of Leibniz Supercomputing Centre Garching (www.lrz.de). Thomas Vogt would like to thank the Korean Ministry of Science, ICT, and Planning (MSIP) for funds associated with a Global Research Laboratory.

REFERENCES

- (1) Breck, D. W. *Zeolite Molecular Sieves: Structure, Chemistry, and Use*; Krieger: Malabar, FL, 1984.
- (2) Dyer, A. *An Introduction to Zeolite Molecular Sieves*; Wiley: Chichester, 1988.
- (3) Ross, M.; Flohr, M. J. K.; Ross, D. R. Crystalline Solution Series and Order-Disorder within the Natrolite Mineral Group. *Am. Mineral.* **1992**, *77*, 685–703.

(4) Alberti, A.; Pongiluppi, D.; Vezzalini, G. The Crystal-Chemistry of Natrolite, Mesolite and Solecite. *Neues Jahrb. Mineral., Abh.* **1982**, *143*, 231–248.

(5) Lee, Y.; Lee, Y.; Seoung, D. Natrolite May Not Be a "Soda-Stone" Anymore: Structural Study of Fully K-, Rb-, and Cs-Exchanged Natrolite. *Am. Mineral.* **2010**, *95*, 1636–1641.

(6) Lee, Y.; Seoung, D.; Lee, Y. Natrolite Is Not a "Soda-Stone" Anymore: Structural Study of Alkali (Li^+), Alkaline-Earth (Ca^{2+} , Sr^{2+} , Ba^{2+}) and Heavy Metal (Cd^{2+} , Pb^{2+} , Ag^+) Cation-Exchanged Natrolites. *Am. Mineral.* **2011**, *96*, 1718–1724.

(7) Lee, Y.; Lee, J. S.; Kao, C. C.; Yoon, J. H.; Vogt, T. Role of Cation-Water Disorder During Cation Exchange in Small-Pore Zeolite Sodium Natrolite. *J. Phys. Chem. C* **2013**, *117*, 16119–16126.

(8) Seoung, D.; Lee, Y.; Kao, C.-C.; Vogt, T.; Lee, Y. Super-Hydrated Zeolites: Pressure-Induced Hydration in Natrolites. *Chem.–Eur. J.* **2013**, *19*, 10876–10883.

(9) Lee, Y.; Seoung, D.; Im, J. H.; Hwang, H. J.; Kim, T. H.; Liu, D.; Liu, Z.; Lee, S. Y.; Kao, C. C.; Vogt, T. Immobilization of Large, Aliovalent Cations in the Small-Pore Zeolite K-Natrolite by Means of Pressure. *Angew. Chem., Int. Ed.* **2012**, *51*, 4848–4851.

(10) Lee, Y.; Liu, D.; Seoung, D.; Liu, Z.; Kao, C.-C.; Vogt, T. Pressure- and Heat-Induced Insertion of CO_2 into an Auxetic Small-Pore Zeolite. *J. Am. Chem. Soc.* **2011**, *133*, 1674–1677.

(11) Lee, Y.; Hriljac, J. A.; Vogt, T.; Parise, J. B.; Edmondson, M. J.; Anderson, P. A.; Corbin, D. R.; Nagai, T. Phase Transition of Zeolite RHO at High-Pressure. *J. Am. Chem. Soc.* **2001**, *123*, 8418–8419.

(12) Kremleva, A.; Vogt, T.; Rösch, N. Monovalent Cation-Exchanged Natrolites and Their Behavior under Pressure. A Computational Study. *J. Phys. Chem. C* **2013**, *117*, 19020–19030.

(13) Lee, Y.; Vogt, T.; Hriljac, J. A.; Parise, J. B.; Artioli, G. Pressure-Induced Volume Expansion of Zeolites in the Natrolite Family. *J. Am. Chem. Soc.* **2002**, *124*, 5466–5475.

(14) Lee, Y.; Hriljac, J. A.; Parise, J. B.; Vogt, T. Pressure-Induced Stabilization of Ordered Paranatrolite: A New Insight into the Paranatrolite Controversy. *Am. Mineral.* **2005**, *90*, 252–257.

(15) Kresse, G.; Hafner, J. Ab Initio Molecular Dynamics for Liquid Metals. *Phys. Rev. B* **1993**, *47*, 558–561.

(16) Kresse, G.; Hafner, J. Ab Initio Molecular-Dynamics Simulation of the Liquid-Metal-Amorphous-Semiconductor Transition in Germanium. *Phys. Rev. B* **1994**, *49*, 14251–14269.

(17) Kresse, G.; Furthmüller, J. Efficiency of Ab-Initio Total Energy Calculations for Metals and Semiconductors Using a Plane-Wave Basis Set. *Comput. Mater. Sci.* **1996**, *6*, 15–50.

(18) Kresse, G.; Furthmüller, J. Efficient Iterative Schemes for Ab Initio Total-Energy Calculations Using a Plane-Wave Basis Set. *Phys. Rev. B* **1996**, *54*, 11169–11186.

(19) Blöchl, P. E. Projector Augmented-Wave Method. *Phys. Rev. B* **1994**, *50*, 17953–17979.

(20) Kresse, G.; Joubert, D. From Ultrasoft Pseudopotentials to the Projector Augmented-Wave Method. *Phys. Rev. B* **1999**, *59*, 1758–1775.

(21) Perdew, J. P.; Burke, K.; Ernzerhof, M. Generalized Gradient Approximation Made Simple. *Phys. Rev. Lett.* **1996**, *77*, 3865–3868.

(22) Perdew, J. P.; Burke, K.; Ernzerhof, M. Erratum: Generalized Gradient Approximation Made Simple. *Phys. Rev. Lett.* **1997**, *78*, 1396–1396.

(23) Poswal, H. K.; Sharma, S. M.; Sikka, S. K. Investigation of Structure and Hydrogen Bonding of Superhydrated Phase B (Ht) under Pressure Using First-Principles Density Functional Calculations. *High Pressure Res.* **2010**, *30*, 198–206.

(24) Le Page, Y.; Saxe, P. Symmetry-General Least-Squares Extraction of Elastic Data for Strained Materials from Ab Initio Calculations of Stress. *Phys. Rev. B* **2002**, *65*, 104104–14.

(25) Shannon, R. Revised Effective Ionic Radii and Systematic Studies of Interatomic Distances in Halides and Chalcogenides. *Acta Crystallogr., Sect. A* **1976**, *32*, 751–767.

(26) Grimme, S. Semiempirical GGA-Type Density Functional Constructed with a Long-Range Dispersion Correction. *J. Comput. Chem.* **2006**, *27*, 1787–1799.

- (27) Jensen, F. *Introduction to Computational Chemistry*, 2nd ed.; Wiley: New York, 2007.
- (28) Halgren, T. A.; Lipscomb, W. N. The Synchronous-Transit Method for Determining Reaction Pathways and Locating Molecular Transition States. *Chem. Phys. Lett.* **1977**, *49*, 225–232.